Electrochemical ELISA-based platform for bladder cancer protein biomarker detection in urine

Sunil K. Arya*[,a], Pedro Estrela*

Centre for Biosensors, Bioelectronics and Biodevices (C3Bio) and Department of Electronic and Electrical Engineering, University of Bath, Claverton Down, Bath BA2 7AY, United Kingdom

[a] Current address: Gwent Electronic Materials Ltd, Monmouth House, Mamhilad Park, Pontypool, Torfaen NP4 0HZ. United Kingdom

---

[*] *Corresponding Authors:* Phone: +44 7405106621, Email: *sunilarya333@gmail.com* (Sunil K Arya), *P.Estrela@bath.ac.uk* (Pedro Estrela)

Abstract

A novel fluidic-based electrochemical ELISA platform is descried for estimation of the bladder cancer protein markers nuclear mitotic apparatus protein 1 (NUMA1) and complement factor H-related 1 (CFHR1). The platform uses an off-site chamber for a sandwich immunoassay and performs the electrochemistry on-chip in a separate chamber. The off-site matrices were connected to the sensor chip in a manner that the sensors were exposed only to the final electroactive product for signal detection, thus avoiding interference from other molecules present in the sample. Two off-site matrices using 3D polymethyl methacrylate (PMMA) sheets and 2D polycarbonate (PC) membranes modified with the desired antibodies were investigated. Antibodies for NUMA1 and CFHR1 were utilized for the immunoassay and hair comb structured gold electrodes were used for sensing. Results in 10% synthetic urine reveal that the system can detect NUMA1 and CFHR1 in the 1–100 ng/ml range with high sensitivities of 260 nA/(ng/ml) and 310 nA/(ng/ml), for NUMA1 and CFHR1, respectively; negligible interference from the diluted urine and other molecules has been observed. A fully automated fluidic prototype has also been developed to demonstrate that automation of the process and multiplexing of detection can be achieved in a small footprint benchtop device. The use of off-site matrix-based platforms paves the way towards a new generation of electrochemical immunosensors for biomarker estimation with negligible non-specific interactions and false signals in complex samples.

Keywords: electrochemical sensor; off-site matrix; PMMA, PC; FNAB; Urine, NUMA1, CFHR1

1. Introduction

Cancer is a life-threatening disease and its various types may affect almost any human organ. Among various cancer types, bladder cancer (BCa) is one of the major cancers affecting around 430,000 people every year worldwide (Ferlay et al., 2013). Bladder's cystoscopic examination along with voided urine cytology (VUC) are the gold standard tests for its preliminary clinical diagnosis (Nakamura et al. 2009; Têtu 2009; Trivedi and Messing 2009). However, cystoscopy, which enables biopsy of doubtful lesions and viewing of bladder lining for histopathological analysis and staging, is invasive, expensive, an uncomfortable procedure and may necessitate anesthetization. VUC testing, on the other hand, which has shown sensitivities in the 13–75% range with specificities in the 85–100% range (Miyake et al. 2012; van Rhijn et al. 2005) depends on microscopic visualization of shed cancer cells in voided urine, and requires trained screeners for assessments. Also, it is non quantitative and has low sensitivity, especially for low-grade tumors (Kumar et al. 2006). Therefore, a wide range of alternative procedures and markers have been proposed and studied for the detection of recurrent bladder tumors. The introduction of non-invasive urine-based markers such as bladder tumor antigen (BTA), nuclear matrix protein 22 (NMP22), along with Immunocyt and fluorescence *in situ* hybridization (FISH), has yielded improved diagnostic accuracy (Parker and Spiess 2011). Also, for better treatment and management of this disease, early detection using non-invasive urine tests are greatly desirable and diagnosis via molecular assays could provide significant advance.

For biomarker-based diagnosis, bladder tumor antigen test involving detection of urinary complement factor H-related proteins (Kinders et al. 1998) and nuclear matrix protein-22 test involving detection of nuclear mitotic apparatus protein 1 (NUMA1) (Miyake et al. 2012) in voided urine samples are most common and FDA approved. However, urinary BTA and NMP-22 tests have shown diagnostic sensitivities in the 29–83% and 47–100% ranges with specificities in the 56–86% and 55–98% ranges, respectively. Thus, more efforts need to be made in order to improve these tests (Grossman et al. 2005; Miyake et al. 2012).

The use of emerging biosensor technology in biomarker detection could be instrumental in early BCa cancer detection, enabling more effective treatments and hence resulting in improvements in patient quality of life and overall chance of survival. Application of biosensors in cancer diagnostics has several advantages over other diagnostic methods including increased assay speed, non-invasive procedure, flexibility, capability for multi-target analysis, automation, and reduced cost of testing (Arya and Bhansali 2011). For BCa diagnosis, estimation of NMP22 and BTA in urine has provided a simple non-invasive way for identifying BCa patients, which is also suitable for the diagnosis and follow-up of BCa cases with high rate of relapse. Till date, for real sample testing, optical enzyme-linked immunosorbent assay (ELISA) has shown great success and is most commonly used method of screening target proteins in real samples (Bettazzi et al. 2012). However, due to its limitation in sensitivity, high cost of instrumentation and non-portability, there is an urgent need to develop new technologies that enable easy screening of high-risk individuals for cancer at an early stage. The combination of immunological techniques with electrochemical detection (electrochemical ELISA) is a promising clinic detection method (Arya et al. 2017a; Arya et al. 2017b) with high sensitivity and specificity, requirement of less time, and low cost. Usually electrochemical ELISA involves the binding of biomolecules and electrochemical signal recognition on the same sensor surface (Kokkinos et al. 2016; Pan et al. 2017; Zhang et al. 2016); however, binding of biomolecules on sensor surfaces may result in degradation of their electrochemical properties and the application of an input electrochemical signal may also affect the sensing layer.

To avoid the mentioned issues and to improve signal sensitivity with low background noise, the present work describes the concept of an integrated sensor chip, where an off-site matrix is employed for on-chip electrochemical biosensing. Two different types of matrices are described to show the utility of the proposed concept as a new biosensor platform. This has been achieved by using a microfluidic based electrochemical platform, where separation of assay chamber and detection chamber with innovative surface chemistry, microfluidic design and electrochemical detection technique has been adopted and

described. The bladder cancer biomarkers NUMA1 and complement factor H-related 1 (CFHR1) have been used as test cases. It should be noted that currently there are no reported biosensors for these two markers. The study is expected to pave way for the development of inexpensive, accurate, and reliable diagnostic devices for bladder specific cancer biomarker detection. Also, a number of biomolecules can be immobilized selectively in an array format to achieve simultaneous multimarker detection and best performance.

2. Materials and Methods

2.1 Chemicals

NUMA1 monoclonal antibody (M01), clone 1C5, NUMA1 human recombinant protein (Q01), glutathione S-transferase (GST) purified rabbit polyclonal antibody, complement factor H-related 1 (CFHR1) recombinant protein (P01), CFHR1 monoclonal antibody (M01), clone 4D7, CFHR1 purified MaxPab rabbit polyclonal antibody (D01P) were purchased from Abnova (Taiwan); goat anti-rabbit IgG H&L (alkaline phosphatase) from Abcam (UK); 4-aminophenyl phosphate monosodium salt (4APP) from Santa Cruz Biotechnology (USA); polycarbonate (PC) membrane filter containing 20 µm holes was procured from Sterlitech (USA); PBS based Starting Block T20 (PBSTSB) from Fisher Scientific (UK); PBST20 from Sigma (UK). 1-fluoro-2-nitro-4-azidobenzene (FNAB) was from Apollo Scientific (UK); synthetic urine from Testclear (USA). Other analytical grade chemicals were utilized as received.

2.2 Gold sensor chips development

Gold sensor chips with a hair comb structure were developed via photolithography patterning and gold deposition technique on silicon oxide coated silicon wafers as described in a previous report (Pui et al. 2013). For the hair comb design, comb fingers of 5 µm width and 3200 µm length with 25 µm spacing were patterned over a length of 5500 µm and connected via a base electrode of 200 µm. Counter gold

electrode and pseudo-reference gold electrode were also deposited on the same chip. The developed hair comb shaped gold sensor chips were washed with ethyl alcohol, acetone and water, and then cleaned using UV-ozone for 30 min before use.

2.3 Formation of PMMA chip and PC membrane and their modification

To make a 3D polymethyl methacrylate (PMMA) chip for the off-site matrix, 11 mm x 12 mm PMMA with 3 mm thickness was laser engraved in an area of 6.5 mm x 7.5 mm to cover the active area of the sensor. Such engraving resulted in the formation of cuboidal pillars (Fig 1a: black dots on white background), thus making 3D structures. Two holes were also made at diagonal end of engraving to create fluidic channel and incubation chamber. Off-site 2D matrix made of poly carbonate (PC) membrane was prepared via laser cutting of large filter into smaller matrix of oval shape with longer width of 9 mm and smaller width of 7 mm (Fig 1b). Prior to FNAB modification, the PMMA matrix was washed and sonicated in IPA for 10 min and then washed using water jet before drying using nitrogen blow. The laser cut membrane was first cleaned with water and methanol following by drying in air. For FNAB modification, 1 mg/25 µl of FNAB in MeOH was found to be optimal as higher concentration resulted in the same response. For 3D PMMA chip and 2D PC membrane, 50 µl and 25 µl solutions, respectively, were found to be enough for complete coverage. The solutions were allowed to dry in dark (Fig 1c and 1d). After drying, the yellow colored matrices were exposed in an UV irradiation system from Oriel Instruments, USA (Fig 1e and 1f: matrix after exposure) and washed with methanol to remove excess FNAB (Fig 1g and 1h). For UV exposure at 75 W power, 30 min minutes were found to be optimum. FNAB during UV exposer resulted in production of highly reactive nitrene group, which underwent grafting on hydrocarbon chain of PMMA/PC surface via covalent bond formation (Bora et al. 2006). Change in color of matrices (Fig 1) suggested successful FNAB modification.

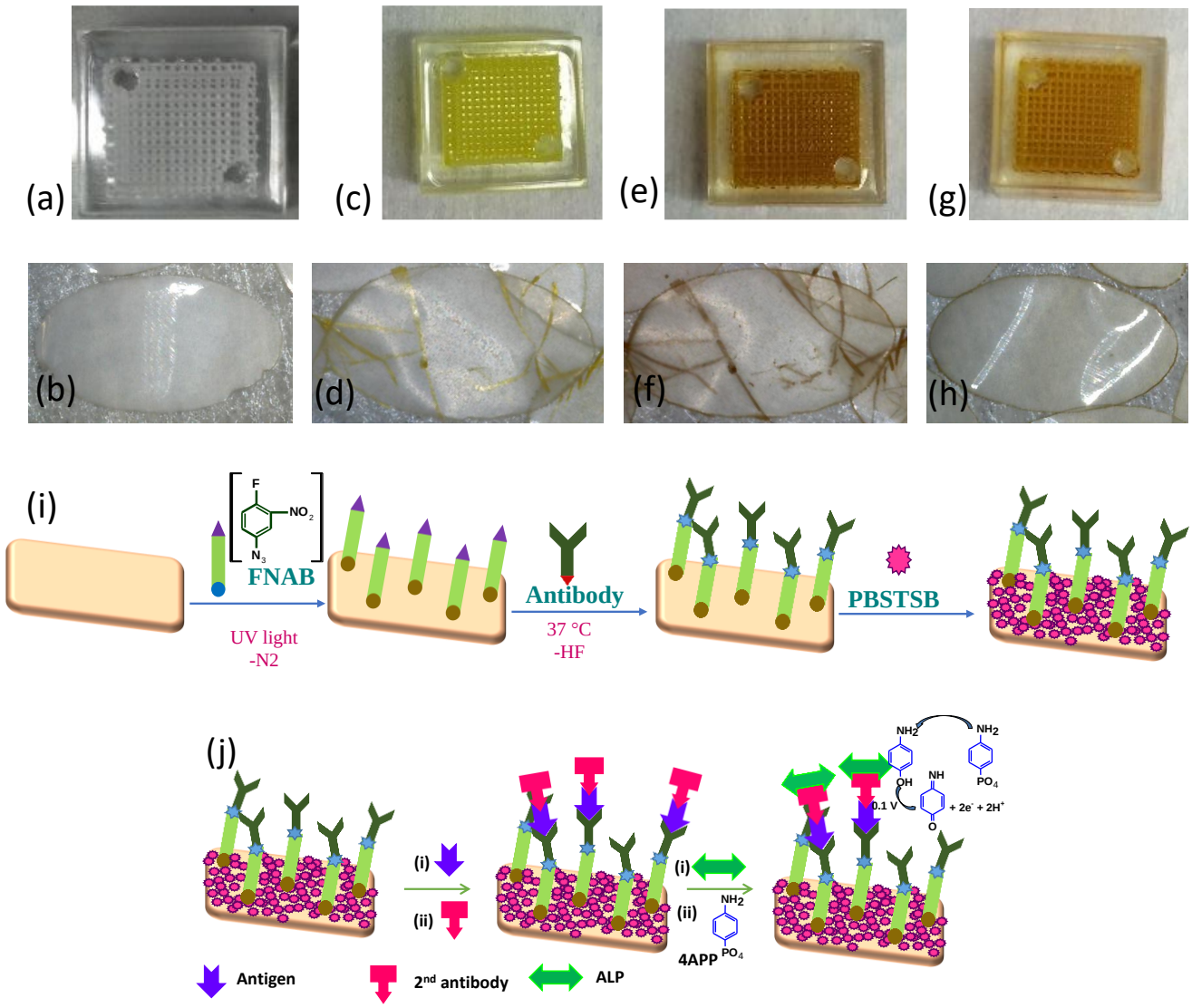

Fig. 1. PMMA/PC matrix at various stages of FNAB modification (a, b) blank laser engraved/cut matrix, (c, d) after dropping FNAB and drying in dark, (e, f) after UV exposure and (g, h) after washing with methanol and drying, (i) schematic for matrix modification and antibody binding, (j) schematic for matrix assembly and bioassay at each step

2.4 Immobilization of antibodies on FNAB modified matrices and chip assembly.

For antibody binding, 5 µg/ml solution of CFHR1 and NUMA1 antibodies were prepared in phosphate buffer (1x) as a stock solution. For covalent immobilization, 50 µl of anti-NUMA1 antibody and 25 µl of anti-CFHR1 antibody solutions in phosphate buffer were dispensed on the PMMA and PC matrices, respectively and were kept at 37 °C for 2 h. During incubation, surface bound FNAB reacts

with the amino groups of antibody and resulted in its covalent binding via nucleophilic replacement reaction on thermally active fluoro group (Arya et al. 2006; Arya et al. 2007; Bora et al. 2006). Antibody modified matrices were washed with PBS tween solution and with PBS to remove physically unbound antibodies. Anti-NUMA1/FNAB/PMMA and anti-CFHR1/FNAB/PC chips were then assembled onto a glass slide using 140 µm thick double side tape and the fluidic connections were made. Incubation for 30 min with PBSTSB blocker was performed for blocking any available free spaces on the matrices. The anti-NUMA1/FNAB/PMMA and anti-CFHR1/FNAB/PC electrodes were thus formed and stored in a humidity chamber in the fridge until use. Figure 1i shows the schematic for matrix modification and antibody binding.

2.5 Sandwich electrochemical immunoassay and signal detection

For antigen detection (NUMA1 on PMMA matrix and CFHR1 on PC matrix), the anti-NUMA1/FNAB/PMMA and anti-CFHR1/FNAB/PC matrices were incubated with desired concentrations of antigen in PBS buffer/10% synthetic urine in PBS. Incubation for 30 min was found sufficient for adequately high and reproducible responses, thus 30 min incubation was used for each step unless otherwise stated. After antigen incubation, the chips were washed with PBST20. The chips were then incubated with 5 µg/ml secondary antibody (from rabbit) solution in PBST20 for 30 min. After incubation, the chips were washed again with PBST20, followed by 30 min incubation with 10 µg/ml alkaline phosphatase (ALP) tagged IgG from rabbit solution in PBST20. After IgG-ALP binding chips were washed with PBST20 and finally incubated with 4APP (2 mg/ml) in 100 mM deoxygenated tris-HCl buffer (pH 9) containing $MgCl_2.6H_2O$ (4 mg/ml) for 20 min followed by differential pulse voltammetric (DPV) signal recording. DPV scan was recorded at step potential of 10 mV, amplitude of 25 mV, and interval time of 0.1 s. DPV scans were performed using Nova 2.1 software on a µAutolab III / FRA2 potentiostat/galvanostat (Metrohm, Netherlands). 10% urine without specific antigen was used as control and 10% urine with non-target antigen or proteins were used for interference studies. All

measurements were repeated on at least three chips and the standard deviation represented via error bars. Fig.1j shows the schematic bioassay at each step.

2.6 Prototype design

Conceptual design for prototype system was made using a microfluidic system with integrated assay and detection chambers (Fig 2b). The prototype was designed to be equipped with a rotating bay to carry reagents, fluidic lines for carrying reagents to assay chamber (Fig 2a) to perform the bioassay, peristaltic pump for controlled speed fluidics valves to control the flow direction, sensor chip for signal detection, control board to control all process automatically and PC to run the program and to display the results. Prototype was designed for handling 4 chips at the same time and multiple assay chambers can be utilized for multiplexing. For biomarker estimation, the assay chamber with specific antibodies was used to capture the desired protein biomarker. A sandwich immunoassay was then programmed with the biomarker and a protein-specific, enzyme labeled detection antibody. In the last step of the assay, added substrate was converted to an electrochemically active form by the enzyme, which is transferred via pump control to the detection chamber, where the electrochemical signal is measured. During processing of all bioassay steps, reagents were flown through the assay chamber and the extra solution was passed to the waste chamber without moving through the detection chamber. In this way the detection chip remained pristine to produce high sensitivity signals with low background noise, thus reducing false positives. Fig. 2 shows the schematic of matrix assembly and prototype concept.

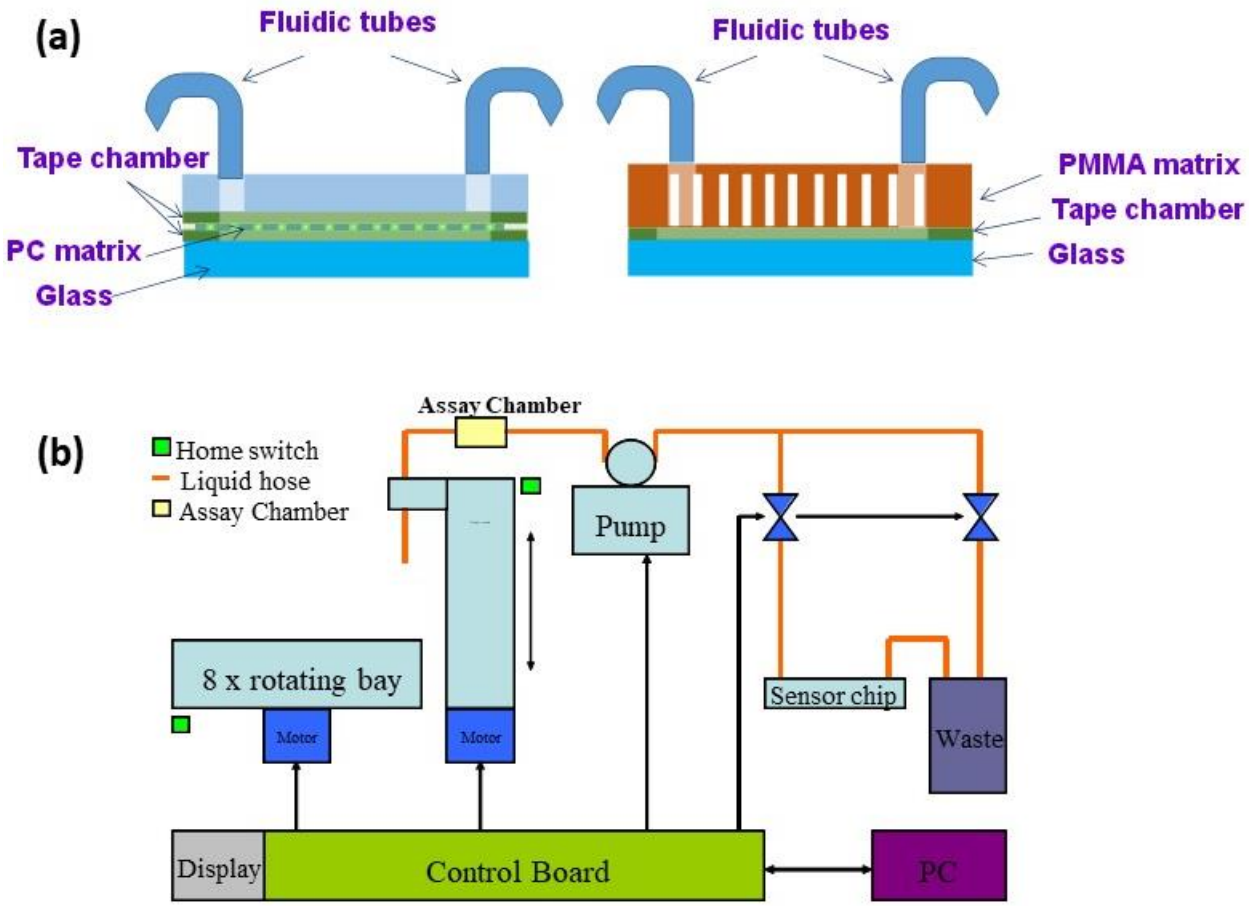

Fig. 2 schematic of (a) PC and PMMA based matrix assembly and (b) prototype concept.

3. Results and discussions

3.1 Off-site matrix with on-chip detection platform and its working principle

Figure 1 shows the general schematic for FNAB based matrix modification and antibody binding along with optical images of 3D laser engraved PMMA and 2D PC matrices at various stages of FNAB modification. The color variation at different stages suggested effective FNAB modification of matrix. For antibody binding, FNAB works as cross-linker and bind to matrix through its azide group and to antibody through its thermally labile fluoro group. Covalent antibody binding via nucleophilic attack by amino group of antibody at reactive thermally labile fluoro group on matrix was achieved at 37 °C (Arya et al. 2006; Arya et al. 2007; Bora et al. 2006). On assembling onto glass surface using double side tape and attached to sensor chip via fluidic tubings, it provided off-site sensor for on-chip detection. Fig. 2

shows the general schematic sensor setup assembly along with the schematic for prototype concept. As immunoassay steps occur on matrix and only final electroactive product was moved to sensor chip, it resulted in better sensitivity and improved reproducibility.

3.2 Blank Gold electrodes with hair comb structure chip characterization and contact angle measurement

Cyclic voltammetry (CV) and electrochemical impedance spectroscopy (EIS) in potassium ferrocynide (5 mM) / potassium ferricynide (5 mM), $[Fe(CN)_6]^{3-/4-}$, in PBS was utilized for characterization of blank gold electrodes with hair comb structures. The CV spectra in Fig 3 show prominent oxidation and reduction peaks with comparable currents and semi reversible behavior, indicating high conductivity and sensitive chip response. Furthermore, 5 different electrodes showed the same CV and EIS responses, indicating a reliable, reproducible fabrication process and can be employed for different concentration on different chip response for comparison.

PMMA/PC matrices at various stages of sensor fabrication were characterized via contact angle measurements (Fig 3c-j) using an in-house built optical angle measurement system (Miodek et al. 2015). For measurement, matrices were placed on the stage using double side tape and a 10 µl of water drop was dispensed on the electrode with the dispensing system. The wetting of surface was then captured using a Nikon p520 camera. Contact angle was measured using a screen protractor version 4.0 procured from Iconico. Fig 3 shows blank PMMA/PC matrix (c, d), after FNAB modification (e, f), after antibody binding (g, h), and after blocking with PBSTSB (i, j). Increase in contact angle value for FNAB modification along with color change indicated successful FNAB binding. Decrease in contact angle value after antibody binding confirms its immobilization and may be attributed to the hydrophilic nature of antibody. Further, decrease in contact angle value after blocking suggested the coverage of hydrophobic free spaces on matrix by hydrophilic proteins present in blocker solution.

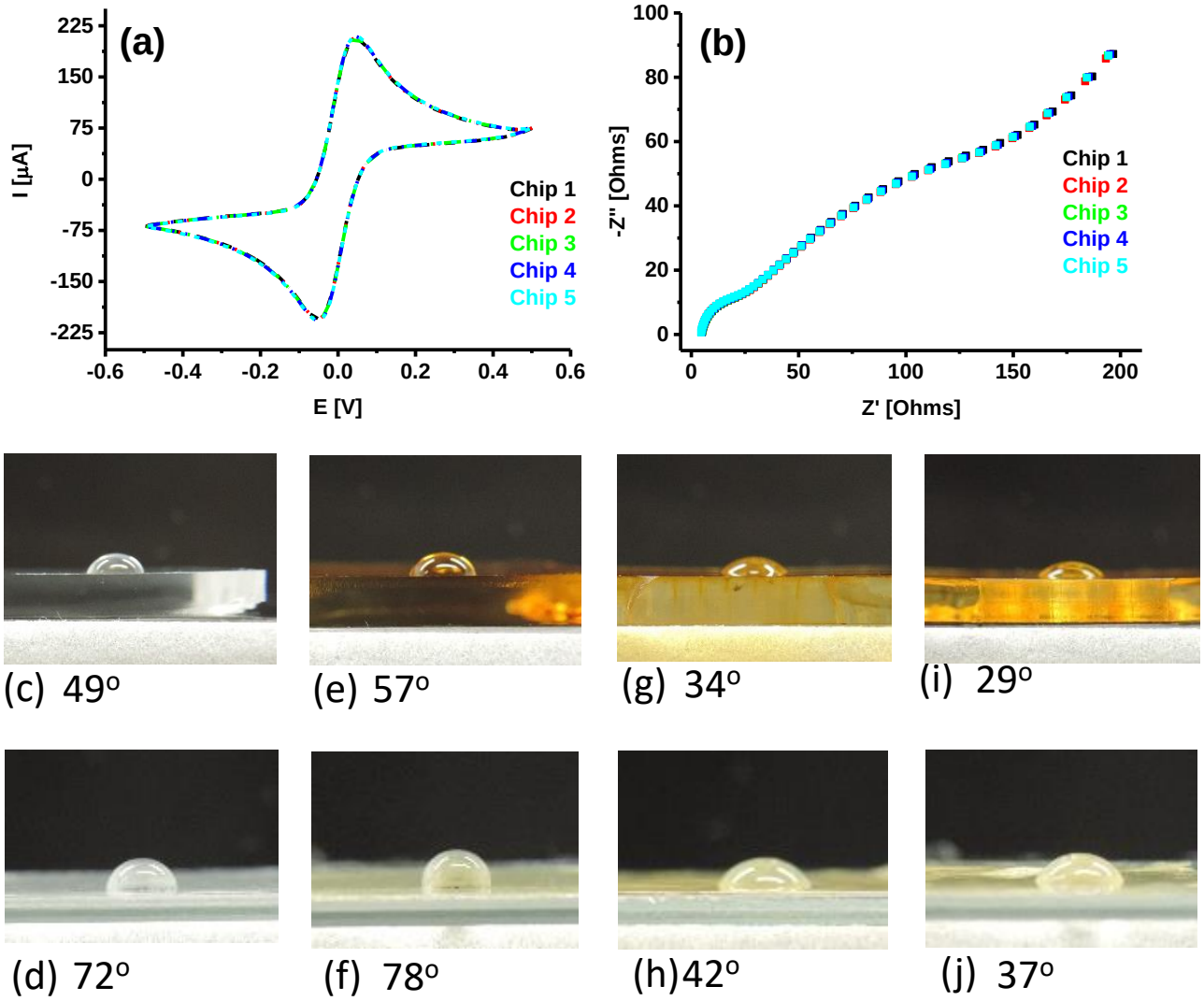

Figure 3. Characterization of blank gold electrodes using (a) CV recording at 50 mV/s scan rate and (b) at EIS. Contact angle images for PMMA/PC matrix at various stages of sensor fabrication blank PMMA/PC matrix (c, d), after FNAB modification (e, f), after antibody binding (g, h), and after blocking with PBSTSB (i, j).

3.3 NUMA1 concentration in PBSTSB *and 10% urine studies on* SB-Anti-NUMA1/FNAB/PMMA electrode

Fig. 4a and 4c show the anti-NUMA1/FNAB/PMMA/glass electrode response for different NUMA1 concentrations (1 ng/ml – 100 ng/ml) in PBSTSB and 10% urine in PBSTSB, respectively, when tested via DPV scans. With increasing concentration, the response current was found to be

increasing, suggesting successful immunoassay. As concentration increases, amount of antigen capture increases, resulting in more secondary antibodies and ALP-IgG molecules binding and resulting in higher production of 4-amino phenol from ALP based conversion of 4APP, which then releases 2 electrons on electrochemical oxidation to quinonimide. Fig. 4b and 4d show the change in current response for different concentrations of NUMA1 in PBSTSB and 10% urine. It is clear that anti-NUMA1/FNAB/PMMA/glass electrode can be used for sensing NUMA1 in buffer and in 10% urine in 1 ng/ml – 100 ng/ml range with sensitivity of 250 nA/(ng/ml), and 260 nA/(ng/ml), respectively and follow linear relationships of ΔI (μA) = 1.2 + 0.25 c_{NUMA1} (ng/ml) and ΔI (μA) = 0.29 + 0.26 c_{NUMA1} (ng/ml) in PBSTSB and in 10% urine, respectively. Error bars representing repeated measurements reveals the consistency within 4% error and the detection limit estimated using 3SD of blank/sensitivity is found to be 1.58 ng/ml and 1.29 ng/ml in PBSTSB and in 10% urine, respectively. Only a slightly higher background signal is observed in urine, while similar variation in peak current and sensitivity suggest that the sensor can be employed in real samples.

To validate the off-site PC matrix based sensor, 2D PC membrane based anti-CFHR1/FNAB/PC/glass electrode was tested for CFHR1 detection also in PBSTSB and in 10% urine. Fig. 5a and 5c show the anti-CFHR1/FNAB/PC/glass electrode response for varying CFHR1 concentrations (1 ng/ml – 100 ng/ml) in PBSTSB and 10% urine, respectively, when tested via DPV scans. Similar to NUMA1, increasing concentration of CFHR1 showed increased response in DPV scans and attributed to increasing concentration of 4-amino phenol from ALP based conversion of 4APP. Fig. 5b and 5d show the change in current response for different concentration of CHRF1 in PBSTSB and 10% urine. It is clear that anti-CFHR1/FNAB/PC/glass electrode can be used for sensing CFHR1 in PBSTSB and urine in the 1 ng/ml – 10 ng/ml range with a sensitivity of 320 nA/(ng/ml) and 310 nA/(ng/ml), respectively and follow linear relationships of ΔI (μA) = 3.36 + 0.32 c_{CFHR1} (ng/ml) and ΔI (μA) = 1.41 + 0.31 c_{CFHR1} (ng/ml) in PBSTSB and in 10% urine, respectively. Error bars representing repeated measurements reveals the consistency within 5% error and the detection limit estimated using

3SD of blank/sensitivity is found to be 1.13 ng/ml and 0.97 ng/ml for CFHR1 in PBSTSB and in 10% urine. Similar to NUMA1, slightly higher background for urine sample suggested some interference from urine contents. Results suggest that measurements for NUMA1 and CFHR1 in urine samples using off site matrix connected to sensor chip via fluidic line based system may provide new and better biosensor platform for measuring of protein markers in urine.

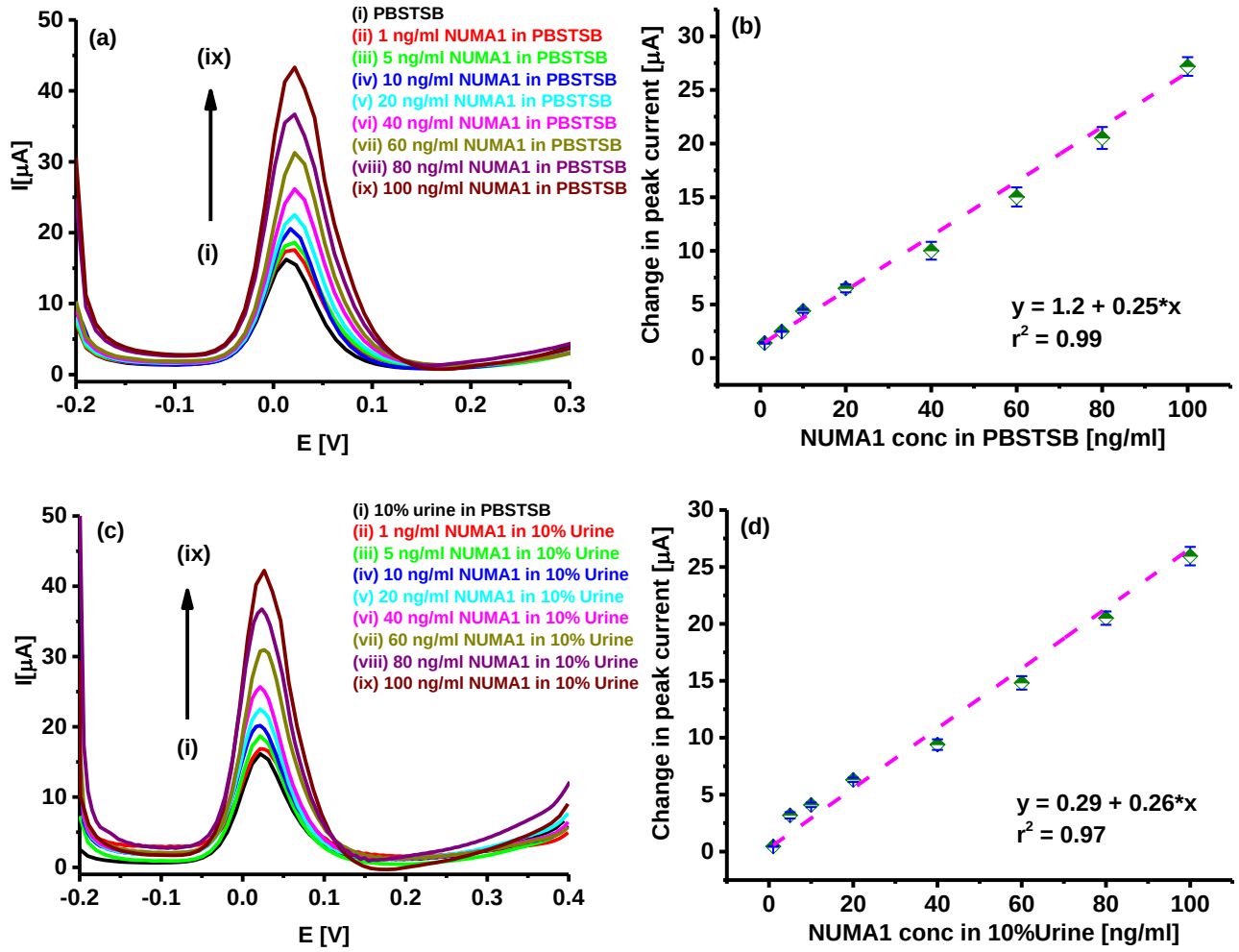

Fig. 4. DPV spectra obtained on anti-NUMA1/FNAB/PMMA matrix for NUMA1 concentrations in (a) PBSTSB, (c) 10% urine in PBSTSB 1 ng/ml–100 ng/ml. NUMA1 concentration linearity curve for normalized current obtained by subtracting blank current value for (b) PBSTSB and (d) 10% urine in PBSTSB.

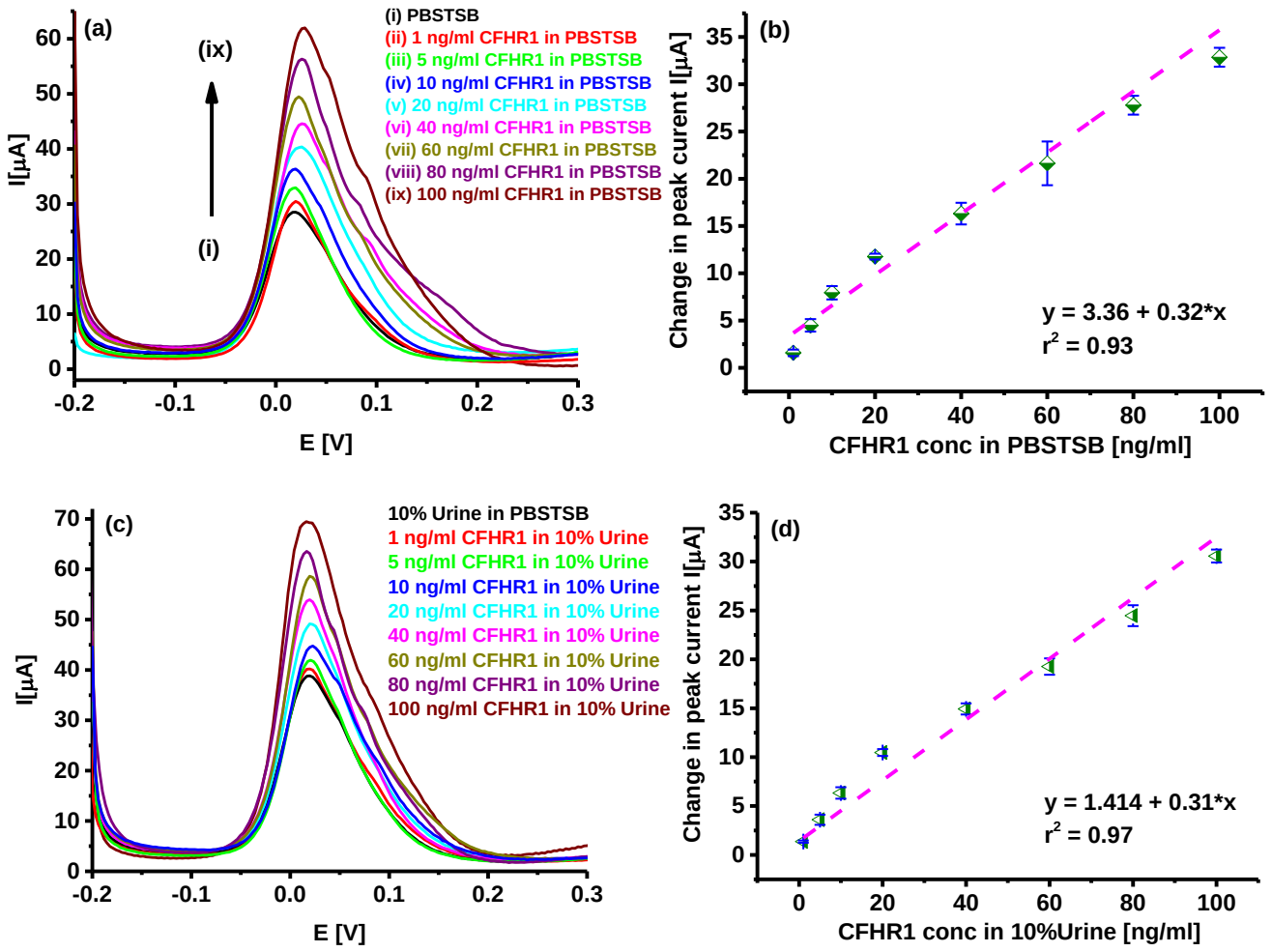

Fig. 5. DPV spectra obtained on anti-CFHR1/FNAB/PMMA matrix for CFHR1 concentrations in (a) PBSTSB, (c) 10% urine in PBSTSB 1 ng/ml–100 ng/ml. CFHR1 concentration linearity curve for normalized current obtained by subtracting blank current value for (b) PBSTSB and (d) 10% urine in PBSTSB.

3.4 Interference studies and prototype response

Anti-NUMA1/FNAB/PMMA/glass electrode was tested for interference from CFHR1, TNF-α and HER2 at concentrations of 100 ng/ml. Fig 6a shows the DPV results, compared with the response with 50 ng/ml NUMA1, i.e. half the concentration of the interferents. Similarly anti-CFHR1/FNAB/PC/glass electrode was tested for interference from NUMA1, TNF-α and HER2 at concentrations of 100 ng/ml and compared with CFHR1 at concentration of 50 ng/ml (Fig 6b). From Fig. 6, it is clear that electrodes do not show significant interference and are specific for their respective

antigen. Further, the electrodes were tested for 3 weeks shelf life at 4 °C and found to show more than 95% response even after three weeks.

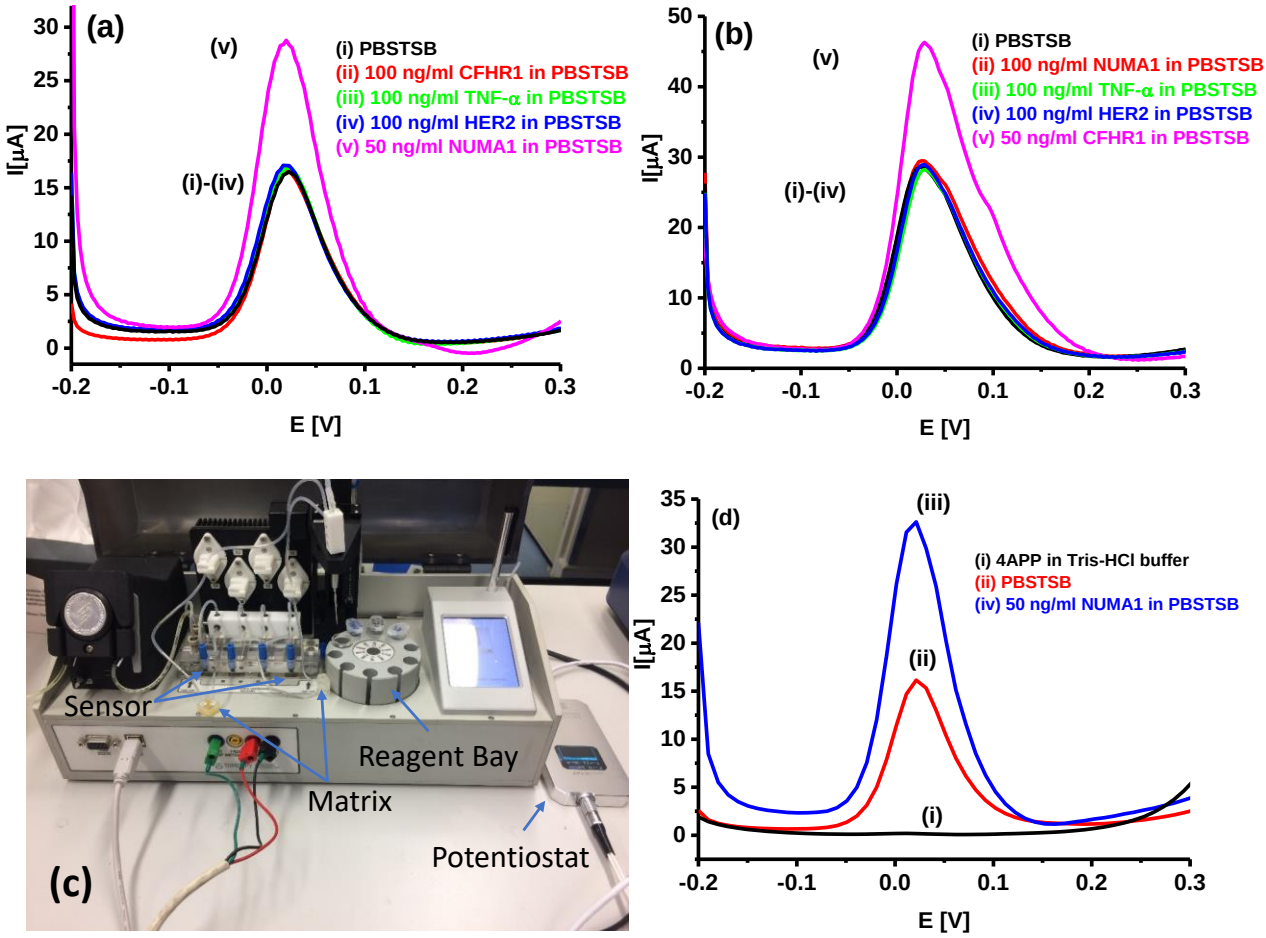

Fig. 6 (a) DPV scans for PBSTSB (i), 100 ng/ml of CFHR1 in PBSTSB (ii), 100 ng/ml of TNF-α in PBSTSB (iii), 100 ng/ml of HER2 in PBSTSB (iv), 50 ng/ml of NUMA1 in PBSTSB (v). (b) DPV scans for PBSTSB (i), 100 ng/ml of NUMA1 in PBSTSB (ii), 100 ng/ml of TNF-α in PBSTSB (iii), 100 ng/ml of HER2 in PBSTSB (iv), 50 ng/ml of CFHR1 in PBSTSB (v). (c) Image of prototype developed and (d) DPV scans for 4APP in Tris-HCl buffer (i) PBSTSB (ii) and 50 ng/ml NUMA1 in PBSTSB (iii).

Using developed procedure and platform, prototype was designed and developed with the help of TOMCOPY Pte Ltd (Fig 6c). The prototype was designed and the software developed in such way that it can control all steps automatically as programmed on display and can run one chip in continuous flow manner or can run multiple chips simultaneously in pulse mode, i.e. it will suck solution from

reagent bay and deliver to matrix with predefined speed and time and then move to 2nd chip for given instruction or wait till incubation period is over before doing 2nd step of assay. Prototype can be run in manual or automatic mode and can be operated directly from its screen or after connected to computer via USB cable and developed software. Further, it can be connected to an electrochemical system such as a potentiostat/galvanostat to run the measurement automatically at the last step via trigger control. During the assay, the solution after each incubation and washing solutions go directly to the waste chamber bypassing the sensor chip; only in the last step the solution from the matrix goes to the sensor chip (controlled delay time and flow rate) and triggers the connected electrochemical system for signal measurement. Initial results for NUMA1 (Fig 6d) suggest that the developed prototype is working as expected and the measurement system can be programmed for simultaneous assays in multiple sensors. To achieve best response from prototype, further optimization for immunoassay using prototype are still required and detailed work is under investigation and finding will be publish in future studies.

4. Conclusions

In conclusion, a fluidic connected off-site matrix based electrochemical ELISA biosensor platform has been developed where the interactions happen in a chamber separate from the sensing electrodes, enabling reduced electrochemical background signal. In validation of developed off-site matrix based platform, antibody-modified sensors exhibited linearity over the 1–100 ng/ml range, with sensitivities of 260 nA/(ng/ml), and 310 nA/(ng/ml), for NUMA1 and CFHR1 respectively in 10% urine samples. Further, electrodes showed detection limits in the diluted urine samples of 1.29 ng/ml and 0.97 ng/ml for NUMA1 and CFHR1, respectively and showed good selectivity during interference studies. The linear ranges are comparable with the more cumbersome standard ELISA kits, which measure CFHR1 in the range 0.78-50 ng/ml and NUMA1 in the range 0.156-10 ng/ml. Although using diluted synthetic urine, the results here presented are extremely promising for the development of sensors for a whole range of protein biomarkers in complex samples.

Furthermore, the use of both 3D PMMA matrix and 2D PC membrane matrix indicate that an off-site matrix based platform can be employed with different types of matrices for wider application. Thus, the proposed system can pave the way for replacement of presently employed optical ELISA systems for biomarker sensing. A prototype has also been made showing electrochemical ELISA for multiple chips, which can be automated and performed easily.

Acknowledgments

S.K.A. was funded by a Marie Skłodowska-Curie Individual Fellowship through the European Commission's Horizon 2020 Programme (grant no. 655176). The prototype was designed and developed with the help of TOMCOPY Pte Ltd.

References

Arya, S.K., Bhansali, S., 2011. Chemical Reviews 111(11), 6783-6809.

Arya, S.K., Kongsuphol, P., Park, M.K., 2017a. Biosensors and Bioelectronics 92, 542-548.

Arya, S.K., Kongsuphol, P., Park, M.K., 2017b. Biosensors and Bioelectronics 91, 721-727.

Arya, S.K., Solanki, P.R., Singh, R.P., Pandey, M.K., Datta, M., Malhotra, B.D., 2006. Talanta 69(4), 918-926.

Arya, S.K., Solanki, P.R., Singh, S.P., Kaneto, K., Pandey, M.K., Datta, M., Malhotra, B.D., 2007. Biosensors and Bioelectronics 22(11), 2516-2524.

Bettazzi, F., Enayati, L., Sánchez, I.C., Motaghed, R., Mascini, M., Palchetti, I., 2012. Bioanalysis 5(1), 11-19.

Bora, U., Sharma, P., Kumar, S., Kannan, K., Nahar, P., 2006. Talanta 70(3), 624-629.

Ferlay, J., Soerjomataram, I., Ervik, M., Dikshit, R., Eser, S., Mathers, C., Rebelo, M., Parkin, D.M., Forman, D., Bray, F., 2013. GLOBOCAN 2012 v1.0, Cancer Incidence and Mortality Worldwide:

IARC CancerBase No. 11. Lyon, France: International Agency for Research on Cancer. Available from http://globocan.iarc.fr, accessed March 2018.

Grossman, H.B., Messing, E., Soloway, M., Tomera, K., Katz. G., Berger, Y., Shen, Y., 2005. JAMA 293(7), 810-816.

Kinders, R., Jones, T., Root, R., Bruce, C., Murchison, H., Corey, M., Williams, L., Enfield, D., Hass, G.M., 1998. Clinical Cancer Research 4(10), 2511.

Kokkinos, C., Economou, A., Prodromidis, M.I., 2016. TrAC Trends in Analytical Chemistry 79, 88-105.

Kumar, A., Kumar, R., Gupta, N.P., 2006. Japanese Journal of Clinical Oncology 36(3), 172-175.

Miodek, A., Regan, E., Bhalla, N., Hopkins, N., Goodchild, S., Estrela, P., 2015. Sensors 15(10), 25015.

Miyake, M., Goodison, S., Giacoia, E.G., Rizwani, W., Ross, S., Rosser, C.J., 2012. BMC Urology 12, 23-23.

Nakamura, K., Kasraeian, A., Iczkowski, K.A., Chang, M., Pendleton, J., Anai, S., Rosser, C.J., 2009. BMC Urology 9(1), 12.

Pan, L.-H., Kuo, S.-H., Lin, T.-Y., Lin, C.-W., Fang, P.-Y., Yang, H.-W., 2017. Biosensors and Bioelectronics 89(1), 598-605.

Parker, J., Spiess, P.E., 2011. The ScientificWorldJournal 11, 1103-1112.

Pui, T.S., Kongsuphol, P., Arya, S.K., Bansal, T., 2013. Sensors and Actuators B: Chemical 181, 494-500.

Siegel, R., Naishadham, D., Jemal, A., 2012. CA: A Cancer Journal for Clinicians 62(1), 10-29.

Têtu, B., 2009. Modern Pathology 22(S2), S53-S59.

Trivedi, D., Messing, E.M., 2009. BMC Urology 9(1), 13.

van Rhijn, B.W.G., van der Poel, H.G., van der Kwast, T.H., 2005. European Urology 47(6), 736-748.

Zhang, Y., Zhang, B., Ye, X., Yan, Y., Huang, L., Jiang, Z., Tan, S., Cai, X., 2016. Materials Science and Engineering: C 59, 577-584.